Alberta Thy 11-06

Large mass expansion in two-loop QCD corrections of para-charmonium decay

K. Hasegawa [1] and Alexey Pak [2]

Department of Physics, University of Alberta,
Edmonton, AB T6G 2J1, Canada

Abstract

We calculate the light-by-light scattering type two-loop QCD corrections due to the light quark loops in the para-charmonium decays $\eta_c \to \gamma\gamma$ and $\eta_c \to gg$. We replace the mass of the internal charm quarks by an artificial large mass and obtain the result as a series in the large mass. The obtained series can be transformed into the good convergent ones by a change of the expansion parameter. The results are supported by two other methods to improve the convergence. We also observe that the color singlet state of η_c eliminates the potential divergences in the two-loop QCD corrections. The obtained corrections to the modes $\eta_c \to \gamma\gamma$ and $\eta_c \to gg$ account for 1.25% and 0.73% of the tree level values, respectively. Comparing the ratio of the decay rates with the experimental value, we find the constrains on the unknown contributions to these decays.

[1] e-mail: hasegawa@phys.ualberta.ca
[2] e-mail: apak@phys.ualberta.ca

1 Introduction

The experimental measurements and the theoretical predictions for the charmonium decays can give us a better knowledge of the standard model parameters. The measurements of the charmonium decays have been continued and improved since the discovery of the ortho-charmonium J/ψ at SLAC and Brookhaven in 1974. In the present paper we focus on the decay modes of the ground-state para-charmonium, $\eta_c \to \gamma\gamma$ and $\eta_c \to gg$. We have two ingredients for the theoretical predictions of the charmonium decays. One is the cross section with the initial state of the charm and anti-charm quarks and the other is a wave function of the charmonium. Since the wave functions are cancelled in the ratio of these decay rates, we here don't deal with the wave function and the corrections to it and we concentrate on the perturbative QCD corrections to the cross section. The one-loop QCD corrections to the decay mode $\eta_c \to \gamma\gamma$ can be obtained from the corrections in the para-positronium (p-Ps) decay into two photons by the trivial replacement of the coupling constants. The one-loop QED corrections to the p-Ps decay are obtained fifty years ago in [1]. After the establishment of QCD, the one-loop QCD corrections to the decay mode $\eta_c \to gg$ are obtained in [2, 3]. The $O(\alpha_s^2)$ corrections to $\eta_c \to \gamma\gamma$ has been discussed in [4]. But the results don't include the light-by-light scattering type corrections. Our purpose in the present paper is to calculate the light-by-light scattering type two-loop QCD corrections due to the light quark loops in the decay modes $\eta_c \to \gamma\gamma$ and $\eta_c \to gg$ which construct a gauge-invariant subset in the all corrections. We first calculate the light-by-light scattering QED corrections to the p-Ps decay. We next adopt the results in the p-Ps decay to the para-charmonium decays and obtain the QCD corrections by counting the color factors mainly.

Multiloop corrections in the perturbative quantum field theory can be calculated by the asymptotic expansion where each loop momentum is factorized into the soft and hard regions [5]. But it is very difficult to calculate the two-loop diagrams in the present paper by the ordinary asymptotic expansions because of the complexity of the diagrams. In order to calculate them we adopt the method of the large mass expansion [6, 7]. We introduce an artificial large mass M and replace the mass of the internal charm quarks by the large mass. We have two mass scales in the diagrams. One is the charm mass of the external charm quarks m_c and the other is the artificial large mass of the internal charm quarks M. We execute the asymptotic expansion with the two mass scales, the soft scale m_c and the hard scale M. When the loop momenta of the internal charm quarks are factorized into the soft scale in the asymptotic expansion, we can expand the propagators of the charm quarks by the ratio m_c/M. The expansions of the propagators transform them into the infinite series of the effective vertices and reduce the original diagrams to the simpler ones which we can calculate. We can obtain the first several terms in the infinite series of m_c/M due to the limited ability of calculation. It is natural that when the expansion parameter m_c/M is much smaller than unity, the series can converge and produce a definite answer. In the present case we must return the artificial mass M to the original one m_c in the end of the calculations. When we set at $M = m_c$ again, it can be caused that the obtained first several terms don't converge and don't produce a definite answer. However we know the origin of the produced series. It is produced by the expansion of the propagators and the series originates in the geometric ones. We can recover the good convergent series by the original analytic information about the series and obtain a definite answer. In the present paper we call the expansions of Feynman diagrams by an artificial large mass "large mass expansion" (LME). We in fact obtain by LME at two-loop level the first several terms which don't seem to converge. An observation of LME at tree level teaches us that a transformation of the expansion parameter can recover a good convergent series. We also check that the results of LME at two-loop level are supported by two other methods to recover the good convergence series, Hölder summation and Shanks transformation [8].

We here overview the roles of the gauge symmetry and the cancellations of the divergences in the two-loop diagrams. We first consider the light-by-light scattering corrections to the p-Ps decay. Since we introduce an artificial mass M in a part of Feynman diagram, we should worry about the gauge symmetry breaking. We can check that the Ward-Takahashi identity [9, 10] does not stand at the tree level and $U(1)_{em}$ gauge symmetry is generally broken in our procedure. But the cross section $\sigma(e^+e^- \to \gamma\gamma)$ contributes to the ground-state p-Ps decay rate in the limits of the electron and positron at rest. We can show that the Ward-Takahashi identity stands in the case that both of the initial electron and positron are rest, which means that the gauge symmetry is restored. We can also expect that the gauge symmetry is kept at the two-loop level under the kinematic situation. We in fact obtain the observables which don't depend on the gauge parameter at the both of the tree and two-loop levels. On the matter of divergences, only the subdiagram of the photon four-point function in the two-loop diagrams has a superficial divergence. Since QED bare lagrangian doesn't have the photon four-point interaction due to the gauge invariance, the subdiagram has no divergence. We don't need renormalization. We next consider the cancellations of the divergences in the two-loop QCD corrections to the para-charmonium decay $\eta_c \to gg$. Only the subdiagram of the gluon four-point function has the superficial divergences and it really diverges because QCD lagrangian has the gluon four-point interactions unlike QED. The divergences must be renormalized by the counter term. In fact if we average the colors of the initial charm and anti-charm quarks over the all possible combinations, the results have divergences. But we can assume that all colors are confined inside hadrons and the all observable hadrons are color singlet state. When we require that the para-charmonium in the initial state is color singlet state, the potential divergences are eliminated and we can obtain the finite results. We can say that the kinematic situation that the initial state is color singlet, which is the dynamical conclusion of QCD, eliminates the potential divergences in the two-loop QCD corrections.

The present paper is organized in the following way. In Sec. 2, we first calculate the tree level decay rate of the p-Ps by two ways, the exact way and LME. We next calculate the light-by-light scattering two-loop QED corrections to the p-Ps decay by LME. We finally check the obtained results by the other two methods. In Sec. 3, we first adapt the results in the p-Ps decay to the para-charmonium decays $\eta_c \to \gamma\gamma$ and $\eta_c \to gg$ and obtain the two-loop QCD corrections by counting the color factors. We next compare the ratio of the two decay rates with the experimental value. In Sec. 4, we have a summary.

2 Positronium decay

Since the two-loop corrections to the para-charmonium decay can be obtained from ones to the p-Ps decay by counting the color factors, we calculate the corrections to the p-Ps

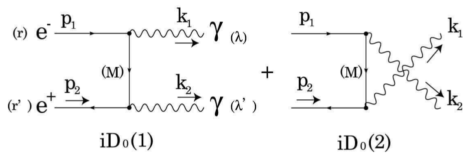

Figure 1: Two diagrams which contribute to the p-Ps decay at tree level are shown.

decay in this section. We can obtain the two-loop corrections by LME. The convergence of the obtained series in LME is not trivial. An observation of the series in LME at tree level teaches us the way to converge the series at two-loop level. For these reasons we first calculate the tree level decay rate of the p-Ps by two ways, the exact way and LME.

Two diagrams contribute to the tree level decay and they are shown in Fig. 1. We replace the electron mass m at the only internal propagators by an artificial large mass M as shown in Fig. 1. The invariant matrix is written as

$$iD_{0\,(r,r',\lambda,\lambda')} = iD_0(1) + iD_0(2) \tag{1}$$

$$= -ie^2\bar{v}^{(r')}(p_2)\left[\gamma_\nu\frac{(\not p_1-\not k_1)+M}{(p_1-k_1)^2-M^2}\gamma_\mu+\gamma_\mu\frac{(\not p_1-\not k_2)+M}{(p_1-k_2)^2-M^2}\gamma_\nu\right]u^{(r)}(p_1)\,\epsilon^\mu_\lambda(k_1)\,\epsilon^\nu_{\lambda'}(k_2)\,; \tag{2}$$

where $u^{(r)}$ and $v^{(r')}$ are the spinors of the electron and positron and ϵ_λ and $\epsilon_{\lambda'}$ are the polarization vectors of the two photons. We average the squared invariant matrix over all polarizations of the external fields and define them as

$$\overline{|D_0|^2} \equiv \frac{1}{4}\sum_{r,r',\lambda,\lambda'}|D_0|^2 \tag{3}$$

$$= \frac{1}{4}\sum_{r,r',\lambda,\lambda'}\left(|D_0(1)|^2+|D_0(2)|^2+D_0(1)D_0^*(2)+D_0^*(1)D_0(2)\right) \tag{4}$$

$$= \overline{|D_0(1)|^2}+\overline{|D_0(2)|^2}+\overline{D_0(1)D_0^*(2)}+\overline{D_0^*(1)D_0(2)}. \tag{5}$$

Each squared invariant matrix is calculated as

$$\overline{|D_0(1)|^2}(x,y) = 2e^4\frac{1}{(m^2-M^2-y)^2}\left[xy+2ym^2-4m^4+2m(M-m)(x-3y-2m^2)+(M-m)^2(x+y-10m^2)\right]; \tag{6}$$

$$\overline{|D_0(2)|^2}(x,y) = \overline{|D_0(1)|^2}(y,x); \tag{7}$$

$$\overline{D_0(1)D_0^*(2)} = \overline{D_0^*(1)D_0(2)} = 2e^4\frac{1}{(m^2-M^2-x)(m^2-M^2-y)}\left[m^2(x+y)-4m^4+4m(M-m)(x+y-m^2)+(M-m)^2(x+y+2m^2)\right]. \tag{8}$$

Here x and y are defined as $x = 2p_1\cdot k_2 = 2p_2\cdot k_1$ and $y = p_1\cdot k_1 = p_2\cdot k_2$. We fix our frame at the center-of-mass one. Since the cross section in the low momentum limit,

$p_1 \to 0$, contributes to the ground-state p-Ps decay, we can use the values, $x = y = 2m^2$. Entering the values into Eqs. (6), (7), and (8), we obtain them as,

$$\overline{|D_0(1)|^2}(x;y)/\alpha_e^2 = \overline{|D_0(2)|^2}(x;y)/\alpha_e^2 = \frac{4r^2}{(1+r^2)^2}(-3+5r^2); \tag{9}$$

$$\overline{D_0(1)D_0^*(2)}/\alpha_e^2 = \overline{D_0^*(1)D_0(2)}/\alpha_e^2 = \frac{4r^2}{(1+r^2)^2}(+3-3r^2); \tag{10}$$

where r is defined as $r \equiv m/M$ and α_e is fine-structure constant. We obtain the total squared matrix as

$$\frac{\overline{|D_0|^2}}{2\alpha_e^2} = \frac{8r^4}{(1+r^2)^2}. \tag{11}$$

Then we obtain the total cross section in the low momentum limit as

$$\sigma_0(e^+e^- \to \gamma\gamma) = \frac{1}{256\pi^2\beta m^2}\frac{1}{2}\int d\Omega\,\overline{|D_0|^2} = \frac{\pi r_0^2}{2\beta}\frac{4r^4}{(1+r^2)^2}; \tag{12}$$

where we write the electron velocity as β and the classical radius of electron as $r_0 \equiv \alpha_e/m$. Using the total cross section, we can also obtain the decay rate of the p-Ps as

$$\Gamma(\text{p-Ps} \to \gamma\gamma) = (2\beta)\cdot 4\sigma_0(e^+e^- \to \gamma\gamma)\cdot|\psi(0)|^2 \tag{13}$$

$$= \frac{m\alpha_e^5}{2}\frac{4r^4}{(1+r^2)^2}; \tag{14}$$

where we use the value of the positronium wave function at the origin, $|\psi(0)|^2 = 1/\pi(2a_0)^3$ with the Bohr radius $a_0 = 1/(m\alpha_e)$. When the artificial mass M is returned to the original electron mass, equally $r = 1$, we obtain the well known p-Ps decay rate at the tree level. In that case the interference terms of the two diagrams, Eq. (10), are vanishing. We have another way to obtain the cross section in Eq. (12). It is the optical theorem. The optical theorem relation in the present decay process can be written as

$$\mathrm{Im}\,M(e^-e^+ \to e^-e^+ : \gamma\gamma) = 4(p_1^0)|\mathbf{p}_1|\,\sigma_0(e^-e^+ \to \gamma\gamma)\times 2; \tag{15}$$

where the left hand side of Eq. (15) is concretely written as

$$(\mathrm{L.H.S}) = \mathrm{Im}\left[2M_1^{\mathrm{tree}} + 2M_2^{\mathrm{tree}}\right]; \tag{16}$$

Two diagrams M_1^{tree} and M_2^{tree} are shown in Fig. 2. If we exactly calculate the left hand side of Eq. (15), we should be able to get the same result with Eq. (12). However we here expand the electron propagators by a large mass M after the Wick rotation before the loop integral as

$$\frac{1}{l^2+M^2} = \frac{1}{M^2}\sum_{n=0}^{\infty}\left(-\frac{l^2}{M^2}\right)^n; \tag{17}$$

where the momentum of the propagator, l, at the only electron mass scale contributes to the imaginary part in Eq. (16) and the scale is assumed to be much smaller than the

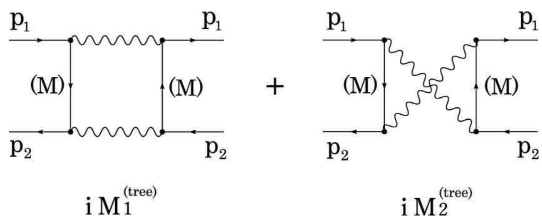

Figure 2: Two diagrams, $M_1^{\rm tree}$ and $M_2^{\rm tree}$, are shown.

artificial large mass M at the present stage. We can not obtain the exact answer including a large mass M at two-loop level and what we can obtain is only a series of r by expanding the propagators as shown in Eq. (17). In order to employ a tree level analysis as a guide for two-loop level, we execute the expansion of propagator at tree level. Further in order to confirm that the gauge symmetry is kept in our calculations, we introduce the gauge parameter ξ in the photon propagator as

$$\langle A_\mu(x)A_\nu(y)\rangle = \int \frac{d^4k}{(2\pi)^4}\frac{-i}{k^2}\left(g_{\mu\nu} + \xi\frac{k_\mu k_\nu}{k^2}\right) e^{-ik\cdot(x-y)} : \tag{18}$$

The cross section is observable and it must not depend on the gauge parameter. We can perform the integration in the left hand side of Eq. (15) using the well known formulae for the massless propagator-type integrals and obtain the following results,

$$\begin{aligned}\frac{\mathrm{Im}\, M_1^{\rm tree}}{\pi\alpha_e^2} &= +r^2(-12-6\xi)+r^3(+24\xi)+r^4(+44+22\xi)+r^5(-80\xi)\\ &\quad + r^6(-76-38\xi)+r^7(+168\xi)+r^8(+108+54\xi)\end{aligned} \tag{19}$$

$$\begin{aligned}\frac{\mathrm{Im}\, M_2^{\rm tree}}{\pi\alpha_e^2} &= +r^2(+12+6\xi)+r^3(-24\xi)+r^4(-36-22\xi)+r^5(+80\xi)\\ &\quad + r^6(+60+38\xi)+r^7(-168\xi)+r^8(-84-54\xi) :\end{aligned} \tag{20}$$

When the exact results (9) and (10) are expanded by r, the series coincide with (19) and (20) with $\xi = 0$ respectively. We sum Eqs. (19) and (20) as

$$\frac{\mathrm{Im}\left(M_1^{\rm tree}+M_2^{\rm tree}\right)}{\pi\alpha_e^2} = +r^4(+8)+r^6(-16)+r^8(+24) ; \tag{21}$$

which does not depend on the gauge parameter as is expected. When the exact result (11) is expanded by r, the series coincides with (21). Here we shed light on the gauge symmetry which seems to be kept in the observable quantity (21). It is possible that to introduce an artificial mass M in a part of Feynman diagrams brakes the $U(1)_{em}$ gauge symmetry. In order to specify the gauge symmetry breaking, we should analyze the Ward-Takahashi identity which is an expression of the gauge symmetries [9, 10]. We extract the one of the polarization vectors of the external two photons from the invariant matrix (2) as follow

$$iD_{0(r,r';\mu,\mu')} \equiv iM_{\mu}(k_1) \tag{22}$$

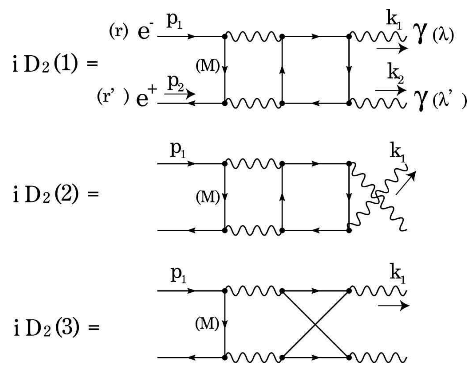

Figure 3: Three diagrams which contribute to the p-Ps decay at two-loop level are shown.

We can observe that the present diagrams which include an artificial mass does not generally satisfy the Ward-Takahashi identity as follow

$$iM^{\mu\nu} k_{1\mu} = -ie^2 \bar{v}^{(r')}(p_2)\left[\frac{(M-m)(\not k_1 \ldots)+\gamma^\nu}{m^2-M^2-y}+\frac{\gamma^\nu (M-m)(\not k_1 \ldots)}{m^2-M^2-x}\right] u^{(r)}(p_1)\,\epsilon_{\lambda'}(k_2) \tag{23}$$

$$\neq 0;$$

which means that the gauge symmetry is broken. However when both of the initial electron and positron are rest in our kinematic situation $p_1 = (m;\vec{0})$ and $p_2 = (m;\vec{0})$, Eq. (23) is simplified into

$$iM^{\mu\nu} k_{1\mu} = ie^2 \frac{M-m}{M^2+m^2} 2k_1^\nu\,\epsilon_{\lambda'}(k_2)\,\bar{v}^{(r')}(p_2)u^{(r)}(p_1) = 0; \tag{24}$$

where we use the relation, $\bar{v}^{(r')}(p_2)u^{(r)}(p_1) = 0$. This means that when the electron and positron are rest, the Ward-Takahashi identity stands and the gauge symmetry is kept. Thus we can justify that the result (21) does not depend on the gauge parameter . Further we can expect that the results at two-loop level should not depend on the gauge parameter.

Here we go to the calculations of the two-loop corrections. We especially calculate the light-by-light scattering corrections shown in Fig. 3. The invariant matrix is written as

$$iD_{(r,r';\lambda,\lambda')} = iD_{0\,(r,r';\lambda,\lambda')} + iD_{2\,(r,r';\lambda,\lambda')}; \tag{25}$$

where the tree level diagrams D_0 and the two-loop level diagrams D_2 are separated into the following diagrams,

$$iD_{0\,(r,r';\lambda,\lambda')} = iD_0(1) + iD_0(2); \tag{26}$$

$$iD_{2\,(r,r';\lambda,\lambda')} = 2\,(iD_2(1) + iD_2(2) + iD_2(3)): \tag{27}$$

Here $D_0(1)$ and $D_0(2)$ are shown in Fig. 1 and $D_2(1)$, $D_2(2)$, and $D_2(3)$ are shown in Fig. 3. In the present paper we restrict the fermions running in the fermion loop to massless ones. Since the electron is the lightest charged fermion, the two-loop corrections are fictional. The light-by-light scattering corrections where the electron runs in the fermion loop are obtained by LME in [11]. The factor 2 in (27) comes from the existence of the diagrams where the rotation of the fermion loop are taken in the inverse direction. Although the inversely directed diagrams are different diagrams from the original ones, the contributions are same. It is worth noting the following two features about the diagrams in Fig. 3. First feature is that the diagrams construct a gauge invariant subset in all two-loop diagrams. This means that the results should not depend on the gauge parameter. Second is that these diagrams have no divergences. The left loop in the two loops has no superficial divergence. Although the right fermion loop has a superficial divergence, it has no divergence because there is no photon four point interaction in QED bare lagrangian due to the gauge symmetry. The diagrams don't need the renormalization and they are calculable. We define the squared and averaged invariant matrices as

$$\overline{|D|^2} \equiv \frac{1}{4}\sum_{r,r';\lambda,\lambda'} |D|^2 = \frac{1}{4}\sum_{r,r';\lambda,\lambda'} \left[|D_0|^2 + D_0 D_2^* + D_0^* D_2 \right] \tag{28}$$

$$\equiv \overline{|D_0|^2} + \overline{D_0 D_2^*} + \overline{D_0^* D_2}. \tag{29}$$

Then we can write the total cross section as

$$\sigma_{tot}(e^+e^- \to \gamma\gamma) = \frac{1}{128\pi m^2}\overline{|D|^2} = \sigma_0 + \Delta\sigma; \tag{30}$$

where the tree level cross section σ_0 and the two-loop corrections $\Delta\sigma$ are written as

$$\sigma_0 = \frac{1}{128\pi m^2}\overline{|D_0|^2}; \tag{31}$$

$$\Delta\sigma = \frac{1}{128\pi m^2}\left[\overline{D_0 D_2^*} + \overline{D_0^* D_2}\right]. \tag{32}$$

We calculate $\Delta\sigma$ through the optical theorem relation at the two-loop level,

$$\mathrm{Im}\, M(e^-e^+ \to e^-e^+;\ \alpha^3) = 4(p_1^0)|\mathbf{p}_1|\,\Delta\sigma(e^-e^+ \to \gamma\gamma) \times 2. \tag{33}$$

The left hand side of the relation (33) can be written as

$$(L.H.S) = 4\,\mathrm{Im}\left[M_1 + M_2 + M_3\right]; \tag{34}$$

where the three-loop diagrams M_1, M_2, and M_3 are shown in Fig. 4. The factor 2 of the factor 4 in Eq. (34) comes from the same origin with the factor 2 in Eq. (27). Another factor 2 comes form the fact that $\overline{D_0 D_2^*}$ in Eq. (32) has six diagrams and three in six are same with the remaining three. The situation is same in the case of $\overline{D_0^* D_2}$. The two loop corrections to the cross section can be expressed through M_1, M_2, and M_3 as

$$\Delta\sigma = \frac{1}{2\pi m^2}\,\mathrm{Im}\left[M_1 + M_2 + M_3\right]. \tag{35}$$

To calculate the corrections (35), we assign an artificial large mass M with the internal electrons as shown in Fig. 4. We have two mass scales in the diagrams, the electron mass

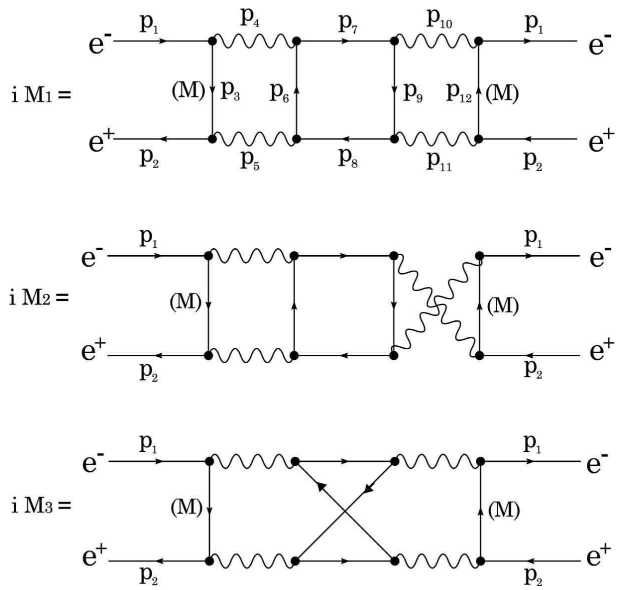

Figure 4: Three diagrams $M_1; M_2$ and M_3 are shown.

m and the artificial large mass M. We execute the asymptotic expansion for the soft scale m and the hard scale M. There are three independent loop momenta in the three-loop diagrams. We can factorize the loop momenta into the soft and hard regions. For example we observe the asymptotic expansion of the diagram M_1. We here take $p_3; p_7;$ and p_{12} as the three independent loop momenta. The diagram M_1 is reduced into the four diagrams which are classified by the soft or hard region of the three loop momenta as shown in Fig. 5. We can obtain $\mathrm{Im}[M_1]$ by summing the four factorized diagrams as follow

$$\mathrm{Im}\ M_1 = \mathrm{Im}\ M_1(r1) + 2 \quad \mathrm{Im} M_1(r2) + 2 \quad \mathrm{Im} M_1(r3) + \mathrm{Im}\ M_1(r4) \; ; \qquad (36)$$

where the factor 2 for $M_1(r2)$ and $M_1(r3)$ comes from the existence of momentum region where the loop momentum p_3 is exchanged with p_{12}. We use FORM [12] for the symbolic manipulations and use the dimensional regularization. The hardest integrals in the region $M_1(r1)$ are calculated using MINCER [13] and the other factorized diagrams are calculated with the well-known formulae for the one- and two-loop integrals. We calculate $\mathrm{Im}[M_1]$ and write the only first two terms as

$$\mathrm{Im}\ M_1 \frac{}{\ ^4} = + \frac{1}{\ } \ ^2 r(+ 6 + 15/2 \quad 12(1 + \ )\log(2r)) \qquad (37)$$

$$+ \frac{1}{\ } \ ^3 r(\ 9 \ + 24 \ \log(2r)) + \qquad ; \qquad (38)$$

where is defined as $= 2 \quad D/2$ in the dimensional regularization. This result depends on the gauge parameter and has the divergences. We can calculate $\mathrm{Im}[M_2]$ in the same

Regions	Reduced diagrams
$M_1(r1): p_3 \ll M,\ p_7 \ll M,\ p_{12} \ll M$	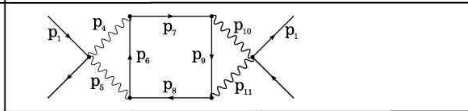
$M_1(r2): p_3 \simeq M,\ p_7 \ll M,\ p_{12} \ll M$	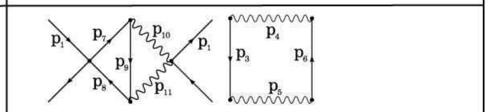
$M_1(r3): p_3 \simeq M,\ p_7 \simeq M,\ p_{12} \ll M$	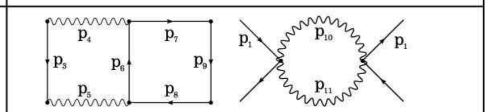
$M_1(r4): p_3 \simeq M,\ p_7 \ll M,\ p_{12} \simeq M$	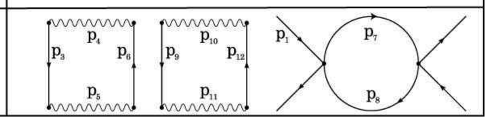

Figure 5: Four regions into which three loop momenta in the diagram M_1 are factorized and the corresponding diagrams into which the diagram M_1 are reduced are shown.

way and obtain the sum of $\mathrm{Im}[M_1]$ and $\mathrm{Im}[M_2]$ up to the first eight terms as

$$
\begin{aligned}
\mathrm{Im}\left[M_1+M_2\right]\frac{\quad}{{}^4} = \; & + r^4\left(-19/6 + 4\log 2r\right) \\
& + r^6\left(+17/3 - 8\log 2r\right) \\
& + r^8\left(-5704/675 + (556/45)\log 2r\right) \\
& + r^{10}\left(+23147/2025 - (2288/135)\log 2r\right) \\
& + r^{12}\left(-19729/1350 + (196/9)\log 2r\right) \\
& + r^{14}\left(+118759/6615 - (1688/63)\log 2r\right) \\
& + r^{16}\left(-10937239/510300 + (453332/14175)\log 2r\right) \\
& + r^{18}\left(+74504699/2976750 - (881504/23625)\log 2r\right); \qquad (39) \\
= \; & \\
& + r^4\left(-0.394078 + 4\log r\right) \\
& + r^6\left(0.121489 - 8\log r\right) \\
& + r^8\left(0.113848 + 12.3556\log r\right) \\
& + r^{10}\left(-0.316944 - 16.9481\log r\right) \\
& + r^{12}\left(0.481131 + 21.7778\log r\right) \\
& + r^{14}\left(-0.618958 - 26.7937\log r\right) \\
& + r^{16}\left(0.734646 + 31.9811\log r\right) \\
& + r^{18}\left(-0.834069 - 37.3123\log r\right). \qquad (40)
\end{aligned}
$$

This result does not depend on the gauge parameter and has no divergences. $\mathrm{Im}[M_3]$ can be also calculated up to the first six terms in the same way and the result is the following,

$$
\begin{aligned}
\mathrm{Im}\ M_3 \quad \frac{}{4} = &\ + \ r^4(\ \ 32/3 + 8 \log 2r + 4\ \ (3)) \\
&+ \ r^6(+20 \quad 16 \log 2r \quad 8\ \ (3)) \\
&+ \ r^8(\ \ 6839/225 + (376/15)\log 2r + 12\ \ (3)) \\
&+ \ r^{10}(+27982/675 \quad (1568/45)\log 2r \quad 16\ \ (3)) \\
&+ \ r^{12}(\ \ 1053506/19845 + (8552/189)\log 2r + 20\ \ (3)) \\
&+ \ r^{14}(+143618/2205 \quad (3536/63)\log 2r \quad 24\ \ (3)) \\
= & \\
&+ \ r^4(\ \ 0.313262 + 8 \log r) \\
&+ \ r^6(\ \ 0.70681 \quad 16 \log r) \\
&+ \ r^8(1.40402 + 25.0667 \log r) \\
&+ \ r^{10}(\ \ 1.93042 \quad 34.8444 \log r) \\
&+ \ r^{12}(2.31841 + 45.2487 \log r) \\
&+ \ r^{14}(\ \ 2.62075 \quad 56.127 \log r); \qquad (41)
\end{aligned}
$$

which has neither of the gauge parameter and the divergence. $\mathrm{Im}\ M_3$ is gauge invariant in itself. We obtain the sum of (40) and (41) as

$$
\begin{aligned}
\mathrm{Im}\ M_1 + M_2 + M_3 \quad \frac{}{4} = &\ + \ r^4(\ \ 0.70734 + 12 \log r) \\
&+ \ r^6(\ \ 0.585321 \quad 24 \log r) \\
&+ \ r^8(1.51786 + 37.4222 \log r) \\
&+ \ r^{10}(\ \ 2.24737 \quad 51.7926 \log r) \\
&+ \ r^{12}(2.79954 + 67.0265 \log r) \\
&+ \ r^{14}(\ \ 3.2397 \quad 82.9206 \log r). \qquad (42)
\end{aligned}
$$

The problem in the results (40), (41), and (42) is that when we set at $r = 1$, the series do not seem to converge and we can not obtain the definite answers at first sight. This situation is similar to the tree level case. The series at tree level in Eq. (21) does not seem to converge at first sight. But when the exact answer (11) are expanded by r, the expanded series coincides with (21). This means that the series (21) with $r = 1$ converges to the limit value, 2, which is given in the exact answer (11) with $r = 1$. The difference between the tree and two-loop levels is that we know the exact answer at the tree level but we don't know it at the two-loop level. We need to recover the exact or the approximate answers from the obtained several terms in Eqs. (40) and (41). The correspondence between the exact answer and the expanded series at the tree level can teach us the way to recover the definite answers at the two-loop level. The way is to change the expansion parameter r into the other one z as follow

$$
z = \frac{2r^2}{1 + r^2}. \qquad (43)
$$

The change of the valuable reconstructs the series of r in Eqs. (40) and (41) into the following series of z,

$$
\begin{aligned}
\mathrm{Im}\, M_1 + M_2 \quad \frac{\ }{4} = \; & + z^2 (\; 0.445093 + 0.5 \log z) \\
& + z^3 (0.166667) \\
& + z^4 (0.0108035 + 0.0111111 \log z) \\
& + z^5 (\; 0.000899527 + 0.00740741 \log z) \\
& + z^6 (\; 0.00156336 + 0.00462963 \log z) \\
& + z^7 (\; 0.00110529 + 0.00297619 \log z) \\
& + z^8 (\; 0.000690984 + 0.00198854 \log z) \\
& + z^9 (\; 0.00042163 + 0.00137743 \log z) + \qquad ;
\end{aligned} \tag{44}
$$

and

$$
\begin{aligned}
\mathrm{Im}\, M_3 \quad \frac{\ }{4} = \; & + z^2 (\; 0.771463 + \log z) \\
& + z^3 (0.333333) \\
& + z^4 (\; 0.00161732 + 0.0333333 \log z) \\
& + z^5 (\; 0.0135782 + 0.0222222 \log z) \\
& + z^6 (\; 0.00839012 + 0.0132275 \log z) \\
& + z^7 (\; 0.00462733 + 0.00793651 \log z) + \qquad :
\end{aligned} \tag{45}
$$

which are good convergent series. Since the series which we can obtain are limited in the first several terms, we should estimate the errors with the remaining infinite series. We can rewrite Eq. (44) as

$$\mathrm{Im}\, M_1 + M_2 \quad \frac{\ }{4} = \sum_{i=2}^{\infty} c_i z^i : \tag{46}$$

After we set at z = 1, equally r = 1, we can neglect log z terms and rewrite as

$$\mathrm{Im}\, M_1 + M_2 \quad \frac{\ }{4} = \sum_{i=2}^{9} c_i + \sum_{i=10}^{\infty} c_i : \tag{47}$$

We can estimate the errors as follow

$$\sum_{i=10}^{\infty} c_i < |c_9| \sum_{i=1}^{\infty} t^i = |c_9| \frac{t}{1 \quad t} : \tag{48}$$

where we can conservatively set at $t = 0.62$ because the ratio $c_9 / c_8 \simeq 0.610$. Considering the negative series, we can obtain the result,

$$
\begin{aligned}
\mathrm{Im}\, M_1 + M_2 \quad \frac{\ }{4} &= \sum_{i=2}^{9} c_i + \frac{1}{2} \frac{t}{1 \quad t} c_9 \quad \frac{1}{2} \frac{t}{1 \quad t} |c_9| && (49) \\
&= 0.2726 \quad 0.00034 \; ({}_{12} d); && (50)
\end{aligned}
$$

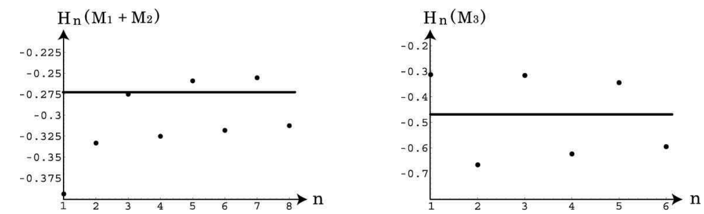

Figure 6: Hölder summation $H_n(M_1+M_2)$ and $H_n(M_3)$ are plotted. The thick lines express the results d_{12} and d_3 in (50) and (51).

where we write this result as d_{12} for the latter references. In the same way, we can obtain the result for $\mathrm{Im}\ M_3$ as

$$\frac{\mathrm{Im}\ M_3}{\pi^4} = -0.4692 \pm 0.0029 \ (\equiv d_3). \tag{51}$$

We obtain the total result by summing (50) and (51) as

$$\frac{\mathrm{Im}\ M_1 + M_2 + M_3}{\pi^4} = -0.7419 \pm 0.0033 \ (\equiv d_{tot}). \tag{52}$$

In order to confirm the results (50) and (51), we estimate the original series (40) and (41) by two other methods, Hölder summation and Shanks transformation [8]. We can recover a good convergence series from a few terms of a slowly convergent or divergent series by these methods if the terms are produced from an analytic function. We first perform Hölder summation. When we have a progression a_n we write the n-th partial sum of the series as $h_n \equiv \sum_{i=1}^{n} a_i$ and Hölder summation is given as

$$H_n \equiv \frac{1}{n}\sum_{i=1}^{n} h_i. \tag{53}$$

We apply the summation to our original results (40) and (41) with $r = 1$ and obtain the summations as,

$$\begin{aligned} H_n(M_1+M_2) &= (-0.394;\ -0.333;\ -0.275;\ -0.325;\ -0.259;\ -0.318; \\ &\qquad -0.255;\ -0.312); \quad (54) \\ H_n(M_3) &= (-0.313;\ -0.666;\ -0.316;\ -0.623;\ -0.344;\ -0.595); \quad (55) \end{aligned}$$

The Hölder summations (54) and (55) are plotted in Fig. 6. We can observe in the plots that the results (50) and (51) are supported by the results of the Hölder summations. Next we try the Shanks transformation. This method also can make the convergence of a series quicker. Shanks transformation is given as

$$S_n \equiv \frac{h_{n-1}h_{n+1} - h_n^2}{h_{n-1} + h_{n+1} - 2h_n}. \tag{56}$$

We can calculate S_n for the original series (40) and (41) as

$$\begin{aligned} S_n(M_1+M_2) &= (1.53;\ -0.242;\ -0.284;\ -0.265;\ -0.277;\ -0.269); \quad (57) \\ S_n(M_3) &= (-0.549;\ -0.428;\ -0.493;\ -0.458); \quad (58) \end{aligned}$$

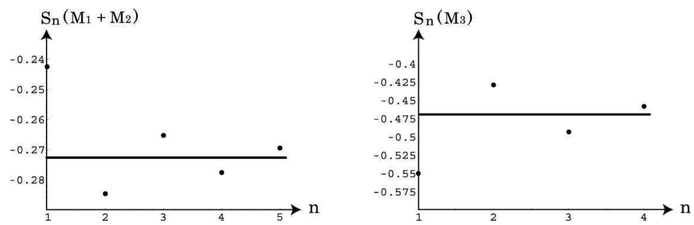

Figure 7: The results in Shanks transformation, $S_n(M_1 + M_2)$ and $S_n(M_3)$, are plotted. The thick lines express d_{12} and d_3.

which are plotted in Fig. 7. The results in this method agree with the results (50) and (51) at the high precision. Thus we can trust the results (50) and (51). Finally to summarize the calculations we write down the obtained fictional corrections to the tree level decay rate as

$$\Gamma(\text{p-Ps} \to \gamma\gamma) = \Gamma_0 \left[1 + \left(\frac{\alpha}{\pi}\right)^2 d_{tot} \right]; \tag{59}$$

where we use Eqs. (12), (13), (35), (52) and the tree level decay rate $\Gamma_0 = m_e \alpha^5/2$.

3 Charmonium decay

We apply the obtained results in Sec. 2 to the ground-state para-charmonium decays $\eta_c \to \gamma\gamma$ and $\eta_c \to gg$ and obtain the light-by-light scattering type two-loop QCD corrections to the decay modes in this section. We first estimate the decay rate of the mode $\eta_c \to \gamma\gamma$. The decay rate can be obtained by the formula like Eq. (13),

$$\Gamma(\eta_c \to \gamma\gamma) = (2\pi)^4 \sigma_{tot}(c\bar{c} \to \gamma\gamma) |\psi_c(0)|^2; \tag{60}$$

where we write the charmonium wave function at the origin as $\psi_c(0)$. The structures of the diagrams which contribute to the tree level decay are the same ones of the diagrams in the p-Ps decay in Fig. 2. The differences between η_c and p-Ps decays are the masses, the electromagnetic charges, and the color factors. We take the differences into consideration and obtain the tree level cross section as

$$\sigma_0(c\bar{c} \to \gamma\gamma) = \sigma_0(e^+e^- \to \gamma\gamma) \left(\frac{m}{m_c}\right)^2 (Q_c)^4 \left(\frac{1}{N_c}\mathrm{Tr}[1]\right)^2 \tag{61}$$

$$= \frac{\pi}{2}\left(\frac{\alpha}{m_c}\right)^2 (Q_c)^4 N_c; \tag{62}$$

where we write the charm mass as m_c, the electromagnetic charge of the charm quark as Q_c, and the number of the kinds of colors as $N_c = 3$. Here 1 is $N_c \times N_c$ unit matrix. The factor $1/N_c$ comes from the color singlet wave function or the state vector of η_c as

$$|\eta_c\rangle = \frac{1}{\sqrt{N_c}} \delta_{ij} |c^i \bar{c}^j\rangle; \tag{63}$$

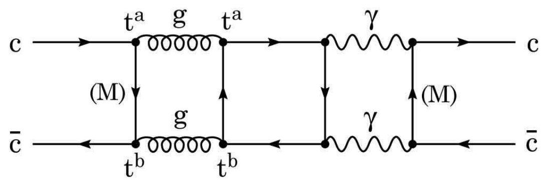

Figure 8: The diagram $M_1(c\bar{c} \to c\bar{c} : \gamma\gamma)$ contributing to the two-loop corrections for the decay $\eta_c \to \gamma\gamma$ is shown. Here g and γ represent the gluon and photon propagators respectively. The diagram corresponds to M_1 in Fig. 4.

where i and j are the color indices of the fundamental representation in the gauge group $SU(3)_{color}$. The factor $Tr[1]^2$ comes from the two color traces which are produced by the requirement of the color singlet state in Eq. (63). Two-loop QCD corrections have the three diagrams corresponding to the three in the p-Ps decay in Fig. 4. One diagram $M_1(c\bar{c} \to c\bar{c} : \gamma\gamma)$ in the three diagrams is shown in Fig. 8, where we write the generators in the fundamental representation as t^a. We restrict the quarks running in the fermion loop to massless ones. Since we can regard the up, down, and strange quarks as massless ones in comparison with the charm quark, the three quarks run in the fermion loop. We obtain $\mathrm{Im}[M_1(c\bar{c} \to c\bar{c} : \gamma\gamma)]$ using $\mathrm{Im}[M_1]$ in the p-Ps decay as

$$\mathrm{Im}\, M_1(c\bar{c} \to c\bar{c} : \gamma\gamma) = \mathrm{Im}\, M_1 \times \left(\frac{\alpha_s}{\alpha_e}\right)^2 (Q_c)^2 [(Q_u)^2 + (Q_d)^2 + (Q_s)^2] \times T_R^2 (N_c^2 - 1); \quad (64)$$

where we write the strong coupling constant as α_s and the the normalization of the generators as $T_R = 1/2$. The factor $T_R^2 (N_c^2 - 1)$ comes from the color trace $Tr[t^a t^b] \times Tr[t^a t^b]$ in Fig. 8. The extracted factors in Eq. (64) are common to the diagram where the rotation of the fermion loop is reversed in Fig. 8 and they are also common to the other two diagrams corresponding to M_2 and M_3 in Fig. 4. Then we can get the two-loop corrections as

$$\Delta\Gamma(c\bar{c} \to \gamma\gamma) = \frac{1}{2\pi m_c^2} d_{tot} \frac{\alpha_e^2 \alpha_s^2}{\pi} (Q_c)^2 [(Q_u)^2 + (Q_d)^2 + (Q_s)^2] \times T_R^2 (N_c^2 - 1); \quad (65)$$

where d_{tot} is defined in (52). Thus we can write the decay rate of $\eta_c \to \gamma\gamma$ including the obtained corrections as

$$\Gamma(\eta_c \to \gamma\gamma) = \Gamma_0(\eta_c \to \gamma\gamma)\left[1 + \frac{\Delta\Gamma}{\Gamma_0}\right] \quad (66)$$

$$= \Gamma_0(\eta_c \to \gamma\gamma)\left[1 + \left(\frac{\alpha_s}{\pi}\right)^2 d_{tot}\right]; \quad (67)$$

where we use Eqs. (62), (65) and the values, $Q_u = Q_c = 2/3$, $Q_d = Q_s = -1/3$, $T_R = 1/2$, $N_c = 3$. We here write the tree level decay rate as

$$\Gamma_0(\eta_c \to \gamma\gamma) = 12\pi \left(\frac{\alpha_e}{m_c}\right)^2 (Q_c)^4 \, |\psi_c(0)|^2 : \quad (68)$$

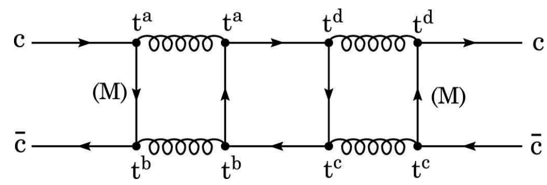

Figure 9: The diagram $M_1(c\bar{c} \to c\bar{c} : gg)$ contributing to the two-loop corrections for the decay $\eta_c \to gg$ is shown. The diagram corresponds to M_1 in Fig. 4.

We next estimate the decay rate of the mode $\eta_c \to gg$. The decay rate can be obtained by the same formula with Eq. (60) as

$$\Gamma(\eta_c \to gg) = (2\pi) \cdot 4\,\sigma_{tot}(c\bar{c} \to gg) \cdot |\psi(0)|^2; \tag{69}$$

The tree level diagrams for this decay are the two diagrams in Fig. 2 where the two photon propagators in each diagram are replaced by the two gluon propagators. We can obtain the tree level cross section as

$$\sigma_0(c\bar{c} \to gg) = \sigma_0(e^+e^- \to \gamma\gamma)\left(\frac{m}{m_c}\right)^2\left(\frac{\alpha_s}{\alpha_e}\right)^2\frac{1}{N_c}\mathrm{Tr}[t^a t^b]\mathrm{Tr}[t^a t^b] \tag{70}$$

$$= \frac{\pi}{2}\left(\frac{\alpha_s}{m_c}\right)^2 2T_R^2 C_F; \tag{71}$$

where we write the Casimir operator in the fundamental representation as $C_F = (N_c^2 - 1)/N_c = 4/3$. Three diagrams which correspond to the three diagrams M_1, M_2 and M_3 in Fig. 4 contribute to the two-loop QCD corrections. One diagram $M_1(c\bar{c} \to c\bar{c} : gg)$ corresponding to M_1 in Fig. 4 is shown in Fig. 9. Using the color singlet wave function in Eq. (63) for η_c, we obtain the common extra factors for M_1 and M_2 in Fig. 4 as

$$\mathrm{Im}\,M_{1,2}(c\bar{c} \to c\bar{c} : gg) = \mathrm{Im}\,M_{1,2} \times \frac{1}{N_c}\mathrm{Tr}[t^a t^b]\mathrm{Tr}[t^c t^d]\mathrm{Tr}[t^a t^b t^c t^d] \times n_q \tag{72}$$

$$= \mathrm{Im}\,M_{1,2} \times T_R^2 C_F^2 n_q; \tag{73}$$

where we write the number of the light quarks as n_q. The color factor for M_3 is different from one for M_1 and M_2, unlike the case of the decay mode $\eta_c \to \gamma\gamma$. We obtain the extra factors for M_3 as

$$\mathrm{Im}\,M_3(c\bar{c} \to c\bar{c} : gg) = \mathrm{Im}\,M_3 \times \frac{1}{N_c}\mathrm{Tr}[t^a t^b]\mathrm{Tr}[t^c t^d]\mathrm{Tr}[t^a t^d t^b t^c] \times n_q \tag{74}$$

$$= \mathrm{Im}\,M_3 \times T_R^2 C_F\left(C_F - \frac{1}{2}C_A\right) n_q; \tag{75}$$

where we write the Casimir operator in the adjoint representation as $C_A = N_c$. Each extracted factor in Eqs. (73) and (75) is same in each diagram where the rotation of the fermion loop is reversed. Using Eqs. (35), (73) and (75) we obtain the two-loop corrections to the cross section as

$$\Delta\sigma(c\bar{c} \to gg) = \frac{1}{2\pi m_c^2}\alpha_s^4 \, T_R^2 C_F\left(C_F d_{tot} - \frac{1}{2}C_A d_3\right) n_q. \tag{76}$$

Then we obtain the decay rate as

$$\Gamma(\eta_c \to gg) = \Gamma_0(\eta_c \to gg)\left[1 + \left(\frac{\alpha_s}{\pi}\right)^2 \frac{n_q}{2}\left(C_F d_{tot} - \frac{1}{2}C_A d_3\right)\right]; \tag{77}$$

where we write the tree level decay rate as

$$\Gamma_0(\eta_c \to gg) = \frac{8}{3}\left(\frac{\alpha_s}{m_c}\right)^2 |\psi(0)|^2 . \tag{78}$$

It should be noted that the cancellations of the divergences between Im M_1 and Im M_2 in the two-loop QCD corrections to the decay $\eta_c \to gg$ are realized by adapting the color singlet wave function in Eq. (63) to η_c. If we average the colors of the charm and anti-charm quarks in η_c over all possible combinations, the divergences are not cancelled and remain because the color factors for M_1 and M_2 are different in that case as

$$\mathrm{Tr}[t^a t^b t^c t^d]\mathrm{Tr}[t^a t^d t^c t^b] \neq \mathrm{Tr}[t^a t^b t^c t^d]\mathrm{Tr}[t^a t^d t^b t^c]. \tag{79}$$

Since the QED bare lagrangian doesn't have the photon four-point interaction due to the gauge invariance, the photon four-point function has no divergence. This fact in QED guarantee that the result (42) has no divergence. On the other hand, the two-loop corrections in Fig. 9 are produced by the interactions in QCD. Since QCD bare lagrangian has the gluon four-point interaction, the gluon four-point function has divergences in proportion to the interaction term in the bare lagrangian. The divergences must be renormalized by the counter term. For these reasons, we don't have any guarantee that the result (76) has no divergence. However, the requirement that the color singlet wave function in Eq. (63) is used for η_c reduces the color factors for M_1 and M_2 from the different ones (79) to the common ones (73). We can conclude that the color confinement for the para-charmonium eliminates the potential divergences in the two-loop QCD corrections.

We estimate what percent the obtained corrections account for in the known predictions of the decay rate. We first estimate the corrections in $\eta_c \to \gamma\gamma$. We can write the general form of the decay rate as

$$\Gamma(\eta_c \to \gamma\gamma) = \Gamma_0(\eta_c \to \gamma\gamma)\left[1 + \frac{\alpha_s}{\pi}\Delta^{(1)} + \left(\frac{\alpha_s}{\pi}\right)^2 \Delta^{(2)}\right]; \tag{80}$$

where the one-loop corrections $\Delta^{(1)}$ is known as $\Delta^{(1)} = (\pi^2 - 20)/3 \simeq -3.38$ [11, 14]. We separate the two-loop corrections into the two parts $\Delta^{(2)} = \Delta_\eta + \Delta^{other}$, where Δ_η is obtained in Eq. (67) as $\Delta_\eta = d_{tot}$ and Δ^{other} is the other two-loop corrections. We use the running coupling constant at the scale of the charm quark mass, $\alpha_s(\mu = m_c) = 0.41$ [15], and obtain the following results,

$$\Gamma(\eta_c \to \gamma\gamma) = \Gamma_0(\eta_c \to \gamma\gamma)\left[1 + (-0.439) + (-0.0125 + 0.017\,\Delta^{others})\right]; \tag{81}$$

where the second and third terms correspond to the one-loop and two-loop corrections respectively. We can find that the obtained two-loop corrections account for -1.25% of the tree level decay rate. Here we neglect the uncertainty of d_{tot} in Eq. (67) due to the smallness. We next estimate the corrections in $\eta_c \to gg$ in the same way. We write the general form of the decay rate as

$$\Gamma(\eta_c \to gg) = \Gamma_0(\eta_c \to gg)\left[1 + \frac{\alpha_s}{\pi}\delta_g^{(1)} + \left(\frac{\alpha_s}{\pi}\right)^2 \delta_g^{(2)}\right]; \tag{82}$$

where the one-loop correction is $\delta_g^{(1)} = \beta_0 \log(\mu/2m_c) + 159/6 - 31\pi^2/24 - 8n_q/9 \simeq 4.87$ [2, 3, 14] with $\mu = m_c$; $\beta_0 = 11 - 2n_q/3$; and $n_q = 3$. We separate the two-loop corrections into the two parts $\delta_g^{(2)} = \Delta_g + \delta_g^{other}$, where Δ_g is obtained in Eq. (77) as $\Delta_g = n_q(C_F d_{tot} - C_A d_3/2)/2$. Then we obtain the results,

$$\Gamma(\eta_c \to gg) = \Gamma_0(\eta_c \to gg)\left[1 + (0.633) + (-0.00729 + 0.017\,\delta_g^{others})\right]. \tag{83}$$

We can find that the obtained corrections account for -0.73% of the tree level. The ratio of the decay rates (82) to (80) is free from the ambiguity and the corrections of the wave function $\psi_c(0)$ and it can give us a rigid prediction. We estimate the ratio as

$$R \equiv \frac{\Gamma(\eta_c \to gg)}{\Gamma(\eta_c \to \gamma\gamma)} = \frac{9}{8}\left(\frac{\alpha_s}{\alpha_e}\right)^2 \frac{1 + (\alpha_s/\pi)\delta_g^{(1)} + (\alpha_s/\pi)^2\delta_g^{(2)}}{1 + (\alpha_s/\pi)\delta_\gamma^{(1)} + (\alpha_s/\pi)^2\delta_\gamma^{(2)}} \tag{84}$$

$$= 1.0 \times 10^4\, \frac{1 + a_g}{1 + a_\gamma}. \tag{85}$$

where we define a_g and a_γ as $a_g = 0.0010\,\delta_g^{others}$ and $a_\gamma = 0.031\,\delta_\gamma^{others}$. When we assume $|a_\gamma| \ll 1$, we can approximate the ratio as

$$R \simeq 1.0 \times 10^4\, [1 + (a_g - a_\gamma)]. \tag{86}$$

As shown in [16], this ratio appears to be sensitive to the scale at which the strong coupling constant is defined. When we use the coupling constant at the scale $\mu = 2m_c$, $\alpha_s(\mu = 2m_c) = 0.28$ [15], the ratio can be estimated as

$$R \simeq 3.4 \times 10^3\, [1 + (a_g - a_\gamma)]; \tag{87}$$

where we define a_g and a_γ as $a_g = 0.0056\,\delta_g^{others}$ and $a_\gamma = 0.011\,\delta_\gamma^{others}$. We can use the experimental value for the ratio R [17] as

$$R^{exp} = (4.0 \pm 1.3) \times 10^3. \tag{88}$$

We plot the theoretical predictions (86) and (87) and the experimental value (88) in Fig. 10. We can read from the plots that if the use of the coupling constant $\alpha_s(\mu = m_c) = 0.41$ is appropriate for the present decays, the difference between the corrections, $a_g - a_\gamma$, must be negative and the magnitude must be larger than about one half and that if the use of $\alpha_s(\mu = 2m_c) = 0.28$ is appropriate, the difference must be smaller than about one half. Conversely we can say also that if the difference $a_g - a_\gamma$ is negative and the magnitude is larger than one half, the use of $\alpha_s(\mu = m_c)$ is favored and that if the magnitude of the difference is smaller than one half, the use of $\alpha_s(\mu = 2m_c)$ is favored.

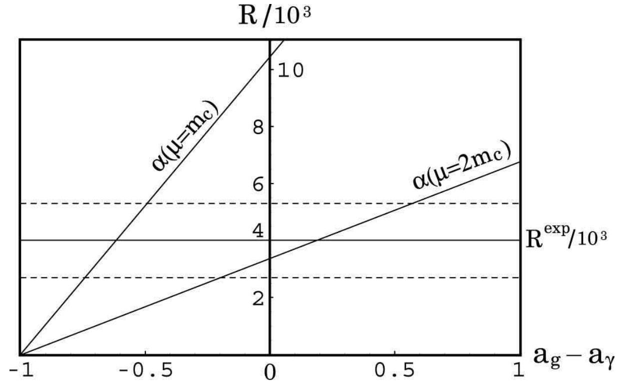

Figure 10: The predictions and experimental value are plotted. Two predictions are given with the two different coupling constants $\alpha_s(\mu = m_c)$ and $\alpha_s(\mu = 2m_c)$. The dashed lines represent the errors with the experimental value R^{exp} in Eq. (88).

4 Summary

We obtain the light-by-light scattering two-loop QED corrections to the p-Ps decay by LME in Sec. 2. We adopt the results in the p-Ps decay to the para-charmonium decays $\eta_c \to \gamma\gamma$ and $\eta_c \to gg$ and obtain the two-loop QCD corrections in Sec. 3, where the massless quarks run in the fermion loop. The use of LME in the two-loop diagrams reduces the original diagrams to the simpler ones which we can calculate. Although the obtained series in LME do not seem to converge, they are transformed into the good convergent ones by the change of the expansion parameter, which is inspired from LME at tree level. We check that the results of the valuable change method are supported by two other methods, Holder summation and Shanks transformation. The light-by-light scattering two-loop QED corrections to the p-Ps decay don't have the divergences due to the gauge invariance. On the other hand, two-loop QCD corrections in the decay mode $\eta_c \to gg$ can have potential divergences because of the gluon four-point self interactions in QCD bare lagrangian. However, we observe that the natural requirement that the para-charmonium η_c is color singlet state eliminates the potential divergences. The obtained two-loop QCD corrections to the decay mode $\eta_c \to \gamma\gamma$ account for 1.25% of the tree level and the corrections to $\eta_c \to gg$ account for 0.73%. We estimate the ratio of the two decay rates, $\Gamma(\eta_c \to gg)/\Gamma(\eta_c \to \gamma\gamma)$, which is free from the ambiguity and the corrections of the charmonium wave function. We obtain two predictions for the ratio which are produced by the two different strong coupling constants $a_s(m_c)$ and $a_s(2m_c)$. The comparison between the predictions and the experimental value gives the constraint on the other unknown corrections. We will be able to do two things to obtain more precise predictions for the decay rates. First is to calculate the other two-loop QCD corrections which are not obtained in the present paper. Second is to specify what strong coupling constant should be used for the present decays. It is also desired that the precision of the experimental value for the ratio will be improved.

Acknowledgements

We are grateful to A. Czarnecki for the suggestion of this subject and the helpful advices. The work of K.H. is supported by the Science and Engineering Research, Canada.

References

[1] I. Harris and L. M. Brown, Phys. Rev. 105 (1957) 1656.

[2] R. Barbieri, G. Curci, E. d'Emilio, and E. Remiddi, Nucl. Phys. B 154 (1979) 535.

[3] K. Hagiwara, C. B. Kim, and T. Yoshino, Nucl. Phys. B 177 (1981) 461.

[4] A. Czarnecki and K. Melnikov, Phys. Lett. B 519 (2001) 212.

[5] M. Beneke and V. A. Smirnov, Nucl. Phys. B 522 (1998) 321.

[6] V. A. Smirnov, Mod. Phys. Lett. A 10 (1995) 1485.

[7] F. V. Tkachev, Sov. J. Part. Nucl. 25 (1994) 649.

[8] C. M. Bender and S. A. Orszag, Advanced Mathematical Methods For Scientists and Engineers, McGraw-Hill, Toronto, (1978).

[9] J. C. Ward, Phys. Rev. 78 (1950) 182.

[10] Y. Takahashi, Nuovo Cim. 6 (1957) 371.

[11] A. Czarnecki, K. Melnikov, and A. Yelkhovsky, Phys. Rev. A 61 (2000) 052502.

[12] J. A. M. Vermaseren, math-ph/0010025.

[13] S. A. Larin, F. V. Tkachov, and J. A. M. Vermaseren, NIKHEF-H-91-18.

[14] W. Kwong, P. B. Mackenzie, R. Rosenfeld, and J. L. Rosner, Phys. Rev. D 37 (1988) 3210.

[15] S. Bethke, Nucl. Phys. Proc. Suppl. 135 (2004) 345.

[16] G. T. Bodwin and Y. Chen, Phys. Rev. D 64 (2001) 114008.

[17] Particle Date Group, W.-M. Yao et al., J. Phys. G 33 (2006) 1.